Accretion rates in hierarchical triple systems with discs

Simone Ceppi, Nicolás Cuello, Giuseppe Lodato, Cathie Clarke, Claudia Toci, Daniel J. Price

Monthly Notices of the ROYAL ASTRONOMICAL SOCIETY

MNRAS **514,** 906–919 (2022) https://doi.org/10.1093/mnras/stac1390
Advance Access publication 2022 May 25

Accretion rates in hierarchical triple systems with discs

Simone Ceppi [1]★ Nicolás Cuello,[2] Giuseppe Lodato [1] Cathie Clarke,[3] Claudia Toci[1] and Daniel J. Price [4]

[1]*Dipartimento di Fisica, Università Degli Studi di Milano, Via Celoria 16, I-20133 Milano, Italy*
[2]*Univ. Grenoble Alpes, CNRS, IPAG, F-38000 Grenoble, France*
[3]*Institute of Astronomy, University of Cambridge, Madingley Road, Cambridge CB3 0HA, UK*
[4]*School of Physics and Astronomy, Monash University, Clayton, VIC 3800, Australia*

Accepted 2022 May 12. Received 2022 May 11; in original form 2021 November 19

ABSTRACT

Young multiple systems accrete most of their final mass in the first few Myr of their lifetime, during the protostellar and protoplanetary phases. Previous studies showed that in binary systems the majority of the accreted mass falls on to the lighter star, thus evolving to mass equalization. However, young stellar systems often comprise more than two stars, which are expected to be in hierarchical configurations. Despite its astrophysical relevance, differential accretion in hierarchical systems remains to be understood. In this work, we investigate whether the accretion trends expected in binaries are valid for higher order multiples. We performed a set of three-dimensional smoothed particle hydrodynamics simulations of binaries and of hierarchical triples (HTs) embedded in an accretion disc, with the code PHANTOM. We identify for the first time accretion trends in HTs and their deviations compared to binaries. These deviations, due to the interaction of the small binary with the infalling material from the circumtriple disc, can be described with a semi-analytical prescription. Generally, the smaller binary of an HT accretes more mass than a single star of the same mass as the smaller binary. We found that in an HT, if the small binary is heavier than the third body, the standard differential accretion scenario (whereby the secondary accretes more of the mass) is hampered. Reciprocally, if the small binary is lighter than the third body, the standard differential accretion scenario is enhanced. The peculiar differential accretion mechanism we find in HTs is expected to affect their mass ratio distribution.

Key words: hydrodynamics – methods: numerical – protoplanetary discs.

1 INTRODUCTION

Surveys of star-forming regions indicate that multiple stellar systems are common in young populations (Duchêne & Kraus 2013; Reipurth et al. 2014). Among Class 0 and Class I stars (younger than 1 Myr), the multiplicity fraction ranges between 40 per cent and 70 per cent (Connelley, Reipurth & Tokunaga 2008; Chen et al. 2013), while in evolved populations, it is around 20 per cent (Duquennoy & Mayor 1991). In addition, molecular cloud simulations show that protostars are likely to form as part of multiple stellar systems and that their surrounding discs experience dramatic dynamical interactions with neighbour stars (Bate 2009, 2018). Thus, multiple stellar systems with discs are expected to be common in star-forming regions. This is also confirmed by surveys of Class 0 systems, as in Tobin et al. (2016).

After the initial collapse of a molecular cloud core, the majority of the mass available to the forming stellar system is confined by angular momentum conservation in the disc and slowly accretes on to the stars (Bonnell & Bate 1994). The tidal torque between the central multiple system and the surrounding disc allows the exchange of angular momentum between the disc and the stellar system (Lin & Papaloizou 1979; Goldreich & Tremaine 1980). The gravitational torque exerted by the multiple system on the circum-multiple disc is thought to suppress the surface density in the surrounding of the stars. Indeed, a high enough angular momentum exchange between the system and the surrounding material is able to open a central cavity in the disc (Artymowicz & Lubow 1996). However, thanks to the asymmetries of the gravitational potential and to the three-dimensional (3D) nature of the problem, accretion of gas on to the stars is not suppressed. Indeed, the stars of the system pull streamers of gas from the inner edge of the cavity. These streamers bridge the lower density region between the disc inner edge and the stellar system allowing the gas to flow towards the stars (Artymowicz & Lubow 1996; Farris et al. 2014; Ragusa, Lodato & Price 2016). There, inner accretion discs around the single stars process the infalling gas that eventually is accreted.

An example is the well-known GG Tauri A (Keppler et al. 2020; Phuong et al. 2020). GG Tau A is a triple (Di Folco et al. 2014) stellar system surrounded by a circumtriple accretion disc. The stars carved a central cavity, where we observe streamers and filaments of gas. Another multiple system that shows cavities and nested discs separated by low-density regions is the GW Orionis triple stellar system (Bi et al. 2020; Kraus et al. 2020). Other similar examples are the binary BHB 2007 (Alves et al. 2019), in which a complex structure of filaments supply gas from the circumbinary disc to the circumstellar discs, and L1448 IRS3B (Reynolds et al. 2021), which is a really young multiple stellar system in formation.

★ E-mail: simone.ceppi@unimi.it

In general, systems with more than two stars are unstable and their evolution eventually leads to the ejection of one body of the system (Valtonen & Karttunen 2006). The only stable configurations observed are made of nested binary orbits and are called hierarchical configurations. For example, a hierarchical triple system is made of a binary orbited at a distance by a third body. In order to preserve the stability of the system, the third body needs to orbit the binary at a distance of several times the binary semimajor axis (see Mardling & Aarseth 2001 for a stability criterion).

How accreting mass from the circum-multiple disc distributes itself around the individual stars plays a key role in the star formation scenario. Indeed, both the evolution of the stellar system masses and the supply of gas around the stars to form inner discs (and possibly inner planets) strongly depend on the competition between the stars in having access to the gas stored in the disc. The study of these processes allows us to also link the properties of the observed evolved population of binaries to their initial conditions in which they initially born (Bate 2000). The fraction of mass accreted by each star of the system depends on the system orbital parameters, in particular on the mass ratio, as shown by Farris et al. (2014). In addition, other less studied system parameters play a role in the mass distribution among the system stars, for example, the infalling gas temperature (Young & Clarke 2015; Young, Baird & Clarke 2015) and the gas viscosity (Duffell et al. 2020).

This process, known as differential accretion, has been widely studied in binaries. Different numerical [smoothed particle hydrodynamics (SPH) and grid] methods show that the secondary star of the binary should accrete most of the disc mass (e.g. in Bate & Bonnell 1997, Farris et al. 2014, and Young et al. 2015). This is due to the lower relative velocity between the secondary and the disc material orbiting at the inner edge, and to the lower distance between the secondary orbit and the inner edge of the disc. However, there are exceptions to this general behaviour when the system orbit is very eccentric. Indeed, in this case, Dunhill, Cuadra & Dougados (2015) showed that discs around binaries with mass ratio lower than unity can temporary accrete more mass on to the primary, and Muñoz & Lai (2016) showed that unitary mass ratio binaries can temporary break the symmetry expected in their accretion rates. Both these exceptions are due to the precession of the eccentric cavity carved by the stellar system.

As of today, however, little is known about differential accretion in hierarchical systems. In this paper, we investigate to which extent the accretion trends of binary systems remain valid for hierarchical triples. In doing so, we propose a model to describe the deviations of the stellar accretion rates in triple systems. We also discuss the possibility to reveal unresolved hierarchical triple systems from their accretion rates and the difficulty in constraining the orbital parameters of the unresolved small binary.

The paper is organized as follows: In Section 2, we describe the systems' setup we considered and their initial conditions. In Section 3, we present our results. We discuss the results of the simulation sets in Section 4, and we give our conclusions in Section 5.

2 HYDRODYNAMICAL SIMULATIONS

We performed gas simulations of coplanar multiple systems embedded in an outer coplanar accretion disc using the 3D SPH code PHANTOM (Price et al. 2018).

We perform three sets of simulations. Set 1 consists of nine simulations made of three binary systems and six hierarchical triple systems. The three binaries have mass ratio $q_{\rm wide} = M_{\rm s}/M_{\rm p} = 0.2, 0.4,$ and 0.65, respectively, where $M_{\rm s}$ is the mass of the lighter star and $M_{\rm p}$ the mass of the heavier one. Initially, the binaries are circular and have a semimajor axis $a_{\rm wide} = 10$ au. From each binary, we derived two hierarchical triple systems. The first kind of triples (labelled *ts*) is built by splitting the secondary star of the binary, while the second kind of triples (labelled *tp*) is built by splitting the primary. In order to build the hierarchical triple systems, the binary stars are split into a circular binary with the same total mass of the split star, with a semimajor axis $a_{\rm small} = 1$ au and a mass ratio $q_{\rm small} = 1$.[1] This set of simulations aims at understanding the effect of the mass ratio on the accretion trends. Table 1 contains the orbital configuration of each of these systems, and Fig. 1 shows the gas surface density after 50 wide binary orbits for each simulation.

Table 1. Hydrodynamical simulation sets. All binary orbits (wider and smaller) are circular and coplanar with the disc. The semimajor axis of each wide orbit is $a_{\rm wide} = 10$ au. All small binaries have a unitary mass ratio $q_{\rm small} = 1$.

Set 1	$\frac{a_{\rm small}}{a_{\rm wide}}$	$q_{\rm wide}$	Split star
*b*2	–	0.2	–
*b*4	–	0.4	–
*b*65	–	0.65	–
*ts*2	0.1	0.2	Secondary
*ts*4	0.1	0.4	Secondary
*ts*65	0.1	0.65	Secondary
*tp*2	0.1	0.2	Primary
*tp*4	0.1	0.4	Primary
*tp*65	0.1	0.65	Primary
Set 2			
*ts*2*a*15	0.15	0.2	Secondary
*ts*2*a*05	0.05	0.2	Secondary
*ts*4*a*18	0.18	0.4	Secondary
*ts*4*a*15	0.15	0.4	Secondary
*ts*4*a*05	0.05	0.4	Secondary
*ts*65*a*20	0.2	0.65	Secondary
*ts*65*a*15	0.15	0.65	Secondary
*ts*65*a*05	0.05	0.65	Secondary
Set 3			
*tp*2*a*20	0.2	0.2	Primary
*tp*2*a*05	0.05	0.2	Primary
*tp*4*a*20	0.2	0.4	Primary
*tp*4*a*05	0.05	0.4	Primary
*tp*65*a*20	0.2	0.65	Primary
*tp*65*a*05	0.05	0.65	Primary

The simulations of Set 2 are devoted to explore the dependence of the triple system accretion rates on the small binary semimajor axis. In Set 2, we consider hierarchical triple systems where we split the secondary star. We start from the *ts*2, *ts*4, and *ts*65 simulations from Set 1, and we vary the small binary semimajor axis as reported in Table 1.

Finally, in Set 3, we focus on hierarchical triple systems where we split the primary star. We start from the *tp*2, *tp*4, and *tp*65 simulations from Set 1, and we vary the small binary semimajor axis as reported in Table 1.

The total stellar mass of each binary and triple system is 3 $M_\odot$. Each system is surrounded by the same coplanar gas disc that initially extends from $R_{\rm in} = 2\,a_{\rm wide}$ to $R_{\rm out} = 10\,a_{\rm wide}$ with a mass equal to

[1] For more information about how we implemented in the PHANTOM code the possibility to simulate hierarchical triple systems, see Appendix B.

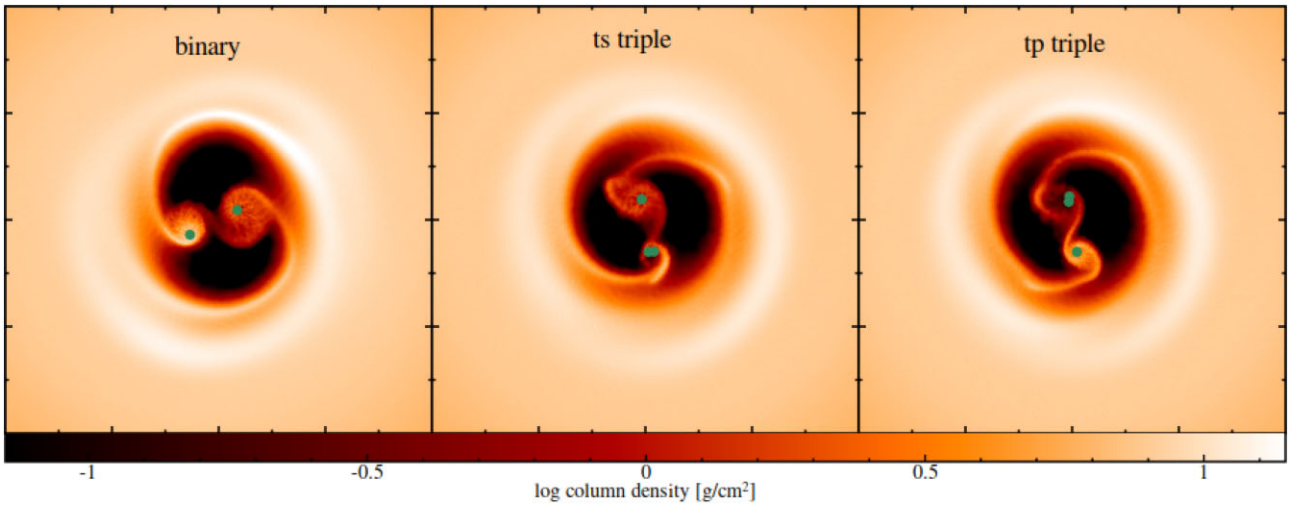

Figure 1. Snapshots of three selected high-resolution simulations of Set 1 showing the gas density in logarithmic scale. Green dots are the sink particles. All the three simulations have $q_{\rm wide} = 0.65$. On the first column, there is the binary. The central column shows the triple system obtained by splitting the secondary star of the binary (*ts* type). On the right column is shown the triple obtained by splitting the primary star of the binary (*tp* type). All snapshots are taken at 55 wide binary orbits.

0.03 $M_\odot$. The disc is modelled using 10^6 SPH particles, resulting in a smoothing length about 0.1 times the disc scale height. The initial gas surface density profile is

$$\Sigma(R) = \Sigma_{\rm in}\left(\frac{R}{R_{\rm in}}\right)^{-p}\left(1-\sqrt{\frac{R_{\rm in}}{R}}\right), \quad (1)$$

with $\Sigma_{\rm in} = 69.4$ g cm^{-2} and $p = 1$. We assume a locally isothermal equation of state centred in the centre of mass of the system. The sound speed profile follows

$$c_{\rm s}(R) = c_{\rm s}(R_{\rm in})\left(\frac{R}{R_{\rm in}}\right)^{-q}, \quad (2)$$

with $q = 0.25$. This results in a disc aspect ratio given by

$$\frac{H}{R} = \frac{H_0}{R_0}\left(\frac{R}{R_{\rm in}}\right)^{(1/2-q)}. \quad (3)$$

We set $H_0/R_0 = 0.1$ at $R = a_{\rm wide}$, as in Farris et al. (2014) and Young & Clarke (2015).

Disc viscosity is implemented via the artificial viscosity method that is standard in SPH (Gingold & Monaghan 1977; Lucy 1977), which can be related to the Shakura & Sunyaev (1973) α-viscosity as found by Lodato & Price (2010). As differential accretion depends on viscosity, we set $\alpha_{\rm SS} = 0.1$, by setting $\alpha_{\rm AV} \approx 9$, to match the values chosen by previous works, in particular by Farris et al. (2014) and Duffell et al. (2020).

Stars are simulated as sink particles (Bate, Bonnell & Price 1995; Price et al. 2018). Sink particles are particles that interact only via gravity with other sink particles and SPH particles. They are evolved via a second-order leapfrog integrator, as described in section 2.8.5 of Price et al. (2018). Sinks are allowed to accrete SPH particles and to store the accreted particles' angular momentum and mass. The accretion of a gas particle can occur when it enters the accretion radius of a sink. To be accreted, the gas particle has to be gravitationally bound to the sink and its angular momentum has to be sufficiently low. In order to reliably resolve the accretion rates, the accretion radius of each sink is set to 0.1 au. This radius is at most ∼0.04 times the wide binary secondary Roche lobe radius, depending on the binary mass ratio (Eggleton 1983).

All our simulations were evolved for 100 wide binary orbits, which correspond to half a viscous time-scale at the disc inner edge $R_{\rm in} \approx 2a_{\rm wide}$, which can be expressed as (Lynden-Bell & Pringle 1974; Hartmann et al. 1998)

$$t_\nu \approx \frac{4}{9}\frac{R^2}{\nu}\bigg|_{R_{\rm in}}, \quad (4)$$

with $\nu = \alpha H c_{\rm s}$. We can write

$$\nu = \alpha H^2 \Omega = \alpha\left(\frac{H}{R}\right)^2 \Omega_{\rm wide}\sqrt{R a_{\rm wide}^3}, \quad (5)$$

where Ω is the Keplerian frequency and $\Omega_{\rm wide}$ is the binary orbital frequency. Using equation (5) at $R = R_{\rm in}$, the viscous time in units of binary orbits is

$$t_\nu|_{R_{\rm in}} \approx \frac{8}{9\sqrt{2}\pi}\frac{1}{\alpha(H/R)^2}\frac{2\pi}{\Omega_{\rm wide}}. \quad (6)$$

With our choice of α and H/R, the viscous time is approximately 200 binary orbits. We discuss the tests we made on longer integration time in Appendix A.

The main observable to be measured in this work is the accretion rate of each star during the simulation. The accretion rates of the simulations conducted in this work are shown in the first row of Figs 2 and 3. We are not interested in the absolute value of the accretion rates but in their ratio. The ratios between the stellar accretion rates cancel out the decreasing trend shown in Figs 2 and 3 because the gas mass distributes with the same proportion between stars, in agreement with what found in Muñoz et al. (2020). In the second row of each mass ratio in Figs 2 and 3, these ratios display a constant trend with an initial transient phase shorter than 20 orbits, showing that differential accretion quickly reaches a steady state.

The accretion rates measured in this work are reported for each orbit, as in Figs 2 and 3. To compute the accretion rates in the nth orbit, we integrate the $\dot{M}(t)$ over the orbital period P, thus

$$\dot{M}_n = \int_{t_n}^{t_n+P}\frac{\dot{M}(t)}{P}{\rm d}t, \quad (7)$$

where t_n is the initial time of the nth orbit. We then averaged with a moving average over 11 orbits (i.e. 4 orbits of the cavity inner edge),

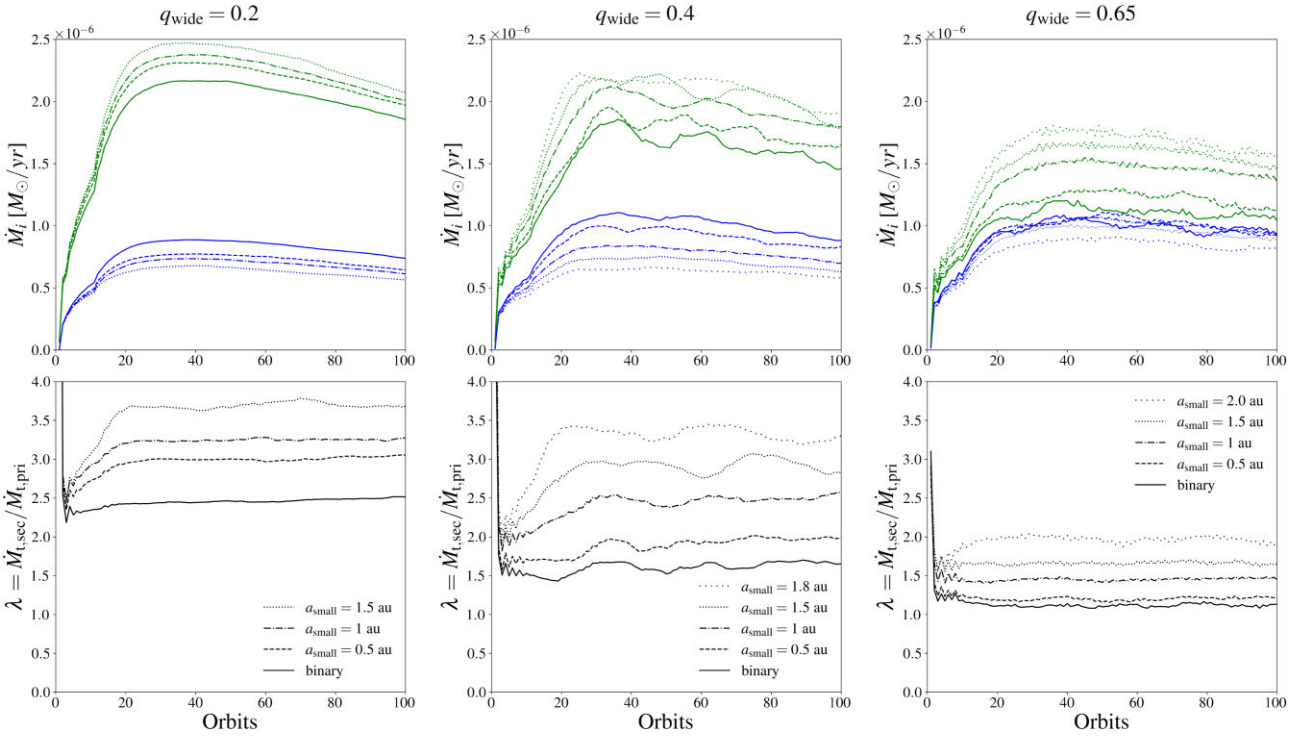

Figure 2. Moving averaged accretion rates and $\lambda = (\dot{M}_{\rm t,sec1} + \dot{M}_{\rm t,sec2})/\dot{M}_{\rm t,pri}$ factors measured in the *ts* triple simulations (Set 2). For each wide orbit mass ratio $q_{\rm wide}$, in the upper panels are plotted the accretion rates of the secondary (green) and primary (blue) star. In the lower panels is plotted the ratio between the accretion rates. The solid line refers to the associated binary, from which the triples are generated. Different line styles refer to different small binary semimajor axes. The secondary accretion rate for the triple system is the sum of the accretion rates of the small binary stars.

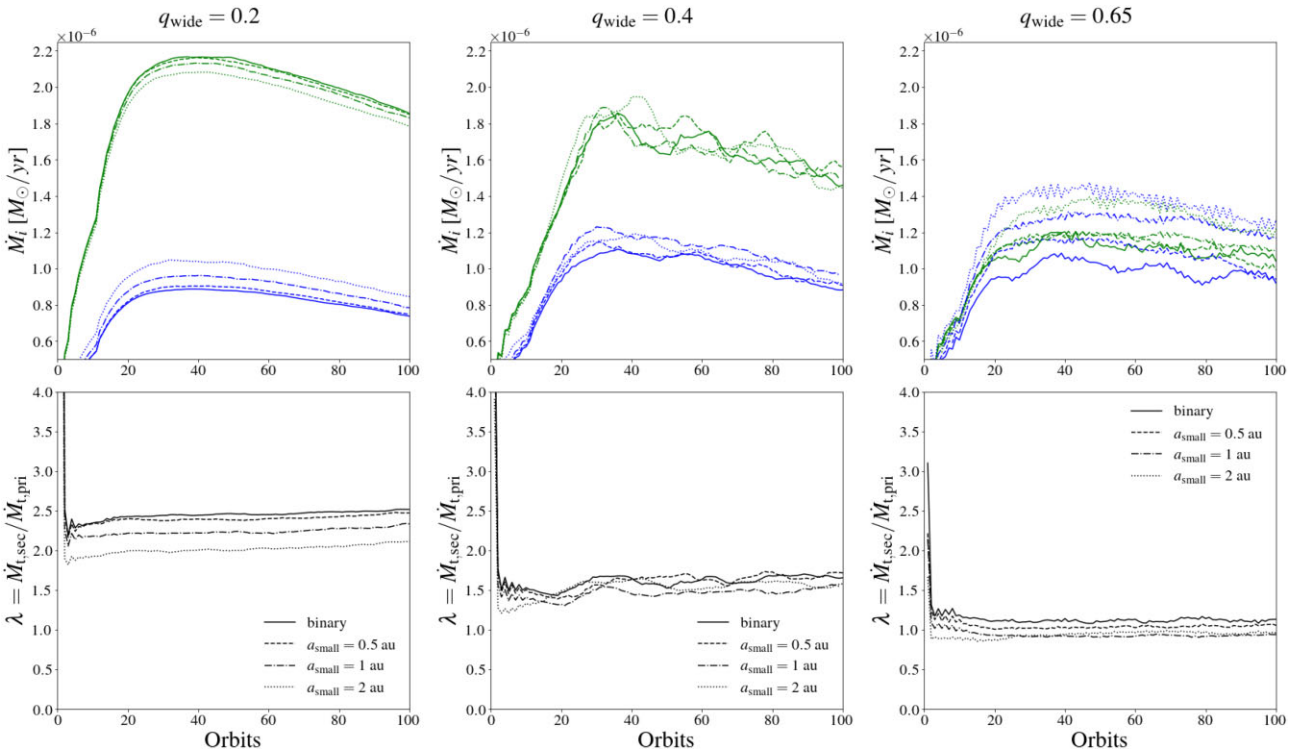

Figure 3. Moving averaged accretion rates and $\lambda = \dot{M}_{\rm t,sec}/(\dot{M}_{\rm t,pri1} + \dot{M}_{\rm t,pri2})$ factors measured in the *tp* triple simulations (Set 3). For each wide orbit mass ratio $q_{\rm wide}$, in the upper panels are plotted the accretion rates of the secondary (green) and primary (blue) star. In the lower panels is plotted the ratio between the accretion rates. The solid line refers to the associated binary, from which the triples are generated. Different line styles refer to different small binary semimajor axes. The primary accretion rate for the triple system is the sum of the accretion rates of the small binary stars.

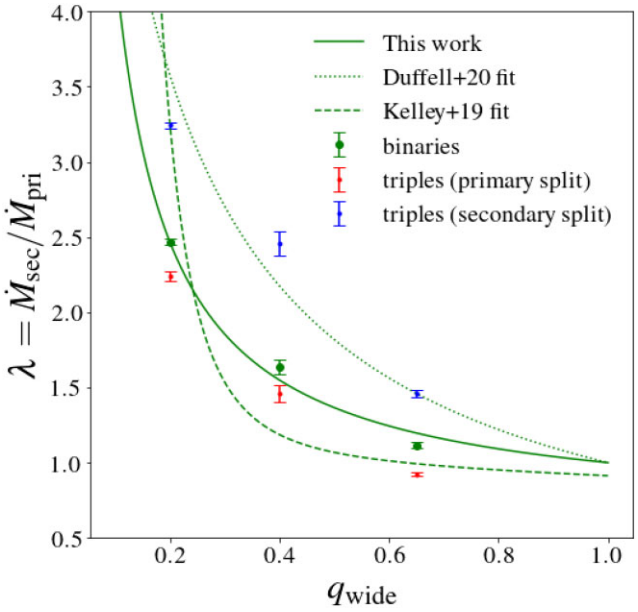

Figure 4. Set 1 simulations' $\lambda = \dot{M}_{\rm sec}/\dot{M}_{\rm pri}$ values. Green dots are binary simulations. Red dots are triples obtained by splitting the primary star of the binary. Blue dots are triples obtained by splitting the secondary star. The solid green curve is the fit proposed in this work in equation (10). Dotted and dashed green curves are the Duffell et al. (2020) and Kelley et al. (2019) parametrizations, respectively.

so that

$$\langle \dot{M}_n \rangle = \frac{\sum_n^{n+10} \dot{M}_i}{11}. \tag{8}$$

The ratios between the stellar accretion rates with their errors (as in Fig. 4) are computed discarding the initial transient orbits.

3 NUMERICAL RESULTS

3.1 Binary systems' differential accretion

The ratio between the stellar accretion rates is the key observable in the binary systems' differential accretion problem. Let us define this factor as

$$\lambda_{\rm b} = \frac{\dot{M}_{\rm b,sec}}{\dot{M}_{\rm b,pri}}, \tag{9}$$

where $\dot{M}_{\rm b,sec}$ and $\dot{M}_{\rm b,pri}$ are the moving averaged accretion rates of the secondary and primary star, respectively (defined in equation 8). The $\lambda_{\rm b}$ ratio measures how evenly the accreting mass distributes over the binary stars. If $\lambda_{\rm b}$ is larger than unity, this means more material is being accreted by the secondary. We simulate three binary systems (with $q_{\rm wide} = 0.2$, 0.4, 0.65, simulations *b*2, *b*4, *b*65) in order to consistently compare the hierarchical triple simulations with their binary counterparts. Fig. 4 shows with green dots the λ factors measured in our Set 1 of 3D SPH binary simulations.

The $\lambda_{\rm b}$ factor depends on the parameters of the system. In particular, $\lambda_{\rm b}$ depends on the mass ratio of the binary, as pointed out by Farris et al. (2014). In addition, $\lambda_{\rm b}$ depends also on the infalling gas properties (Young & Clarke 2015; Young et al. 2015). For a given mass ratio, warmer discs raise the primary accretion rate, pushing $\lambda_{\rm b}$ towards unity. This is due to the fact that warmer gas streamers have a wider range of trajectories to reach the primary star. In addition, warmer gas around the secondary star crosses the Roche lobe more easily, reaching the primary Roche lobe. Lastly, Duffell et al. (2020) showed that $\lambda_{\rm b}$ depends also on gas viscosity. In particular, they found that for less viscous discs, the value of $\lambda_{\rm b}$ tends towards unity.

Recently, two parametrizations for $\lambda_{\rm b}(q)$ were proposed. The first one in Kelley et al. (2019, hereafter K19 parametrization), which updates the one proposed by Gerosa et al. (2015) and is built by fitting the Farris et al. (2014) binary simulation set. The second one in Duffell et al. (2020, hereafter D20 parametrization), who simulate binary accretion discs slowly modifying the binary mass ratio during the simulation in order to span $\lambda_{\rm b}(q)$ continuously. These works, based on different 2D grid numerical techniques, resulted in two different parametrizations (see green curves in Fig. 4). In order to be able to compare our binary simulations with the D20 and K19 parametrizations, we used the same disc thickness and viscosity of previous works, even if higher than the typical protostellar disc viscosity (Hartmann et al. 1998; Dullemond et al. 2018).

As shown in Fig. 4, our binary simulations are in fairly good agreement with the parametrizations proposed in the literature. In particular, we found the same accretion trends described by previous works. Indeed, the secondary star always accretes most of the mass. Moreover, the higher the binary mass ratio, the lower the value of $\lambda_{\rm b}$ (as expected). In addition, if we reduce the thickness of our disc, $\lambda_{\rm b}$ tends to the D20 parametrization. The discrepancies can be due to the different numerical technique we used. In particular, our simulations are 3D as opposed to the 2D ones by Duffell et al. (2020) and Farris et al. (2014), and the disc height profile could vary between simulations away from the inner cavity edge.

We fit our binary data points with the following one-parameter function:

$$\lambda_{\rm b} = C + \frac{1-C}{q_{\rm wide}}, \tag{10}$$

which accounts for the $q_{\rm wide}^{-1}$ dependence found in previous studies (Gerosa et al. 2015; Duffell et al. 2020) and which approaches unity when $q_{\rm wide}$ approaches unity. Indeed, for symmetry reasons, we expect a unitary mass ratio binary to evenly accrete mass on to the two binary stars. Our best fit for the C parameter results in $C = 0.63$. Contrary to K19 and D20 parametrizations, our formula is obtained from a set of 3D simulations, and it is shown in Fig. 4 (green solid curve).

3.2 Hierarchical triples' differential accretion

For a quantitative comparison with the $\lambda_{\rm b}$ factor measured in binaries, we introduce an analogous ratio for hierarchical triples: $\lambda_{\rm t}$. If the small binary of the triple system is lighter than the single body (i.e. in the *ts* type triples), we define $\lambda_{\rm t}$ as the ratio between the sum of the accretion rates of the small binary stars ($\dot{M}_{\rm t,sec1} + \dot{M}_{\rm t,sec2}$) over the accretion rate of the single star ($\dot{M}_{\rm t,pri}$):

$$\lambda_{\rm t} = \frac{\dot{M}_{\rm t,sec1} + \dot{M}_{\rm t,sec2}}{\dot{M}_{\rm t,pri}}. \tag{11}$$

If instead the small binary is heavier than the single body (i.e. in the *tp* triple case), we define $\lambda_{\rm t}$ as the ratio between the accretion rate of the single star ($\dot{M}_{\rm t,sec}$) over the sum of the accretion rates of the small binary stars ($\dot{M}_{\rm t,pri1} + \dot{M}_{\rm t,pri2}$):

$$\lambda_{\rm t} = \frac{\dot{M}_{\rm t,sec}}{\dot{M}_{\rm t,pri1} + \dot{M}_{\rm t,pri2}}. \tag{12}$$

In other words, the $\lambda_{\rm t}$ factor of a hierarchical triple system is defined considering the system as a binary in which the small binary is

treated as a single body, with an accretion rate equal to the sum of the accretion rate of the small binary stars.

Accordingly, we define $q_{\rm wide}$ (the mass ratio of the wide orbit) for the *ts* and the *tp* triple cases. In the former case, we define

$$q_{\rm wide} = \frac{M_{\rm t,sec1} + M_{\rm t,sec2}}{M_{\rm t,pri}}, \tag{13}$$

where $M_{\rm t,\,sec1}$ and $M_{\rm t,\,sec2}$ are the mass of the small binary primary and secondary, respectively, and $M_{\rm t,\,pri}$ is the mass of the single body. In the latter case, we define

$$q_{\rm wide} = \frac{M_{\rm t,sec}}{M_{\rm t,pri1} + M_{\rm t,pri2}}, \tag{14}$$

where $M_{\rm t,\,pri1}$ and $M_{\rm t,\,pri2}$ are the mass of the small binary primary and secondary, respectively, and $M_{\rm t,\,sec}$ is the mass of the single body. In Fig. 4, we show, for each $q_{\rm wide}$ in Set 1, the $\lambda_{\rm t}$ factors of the triple simulations, along with the $\lambda_{\rm b}$ factor of their associated binaries.

The differential accretion in hierarchical triple is set by the combination between the binary differential accretion and the effects induced by the presence of the small binary. Thus, in order to isolate the contributions of the small binary to differential accretion, we compared each hierarchical triple simulation with its associated binary. In order to do this, we associated with each binary system discussed in Section 3.1 (i.e. each *b* simulation) two hierarchical triple systems, obtaining the nine simulations of Set 1 (see Table 1). The two associated triples are built by substituting the primary or the secondary binary star with a small binary, obtaining, respectively, the *tp* and *ts* triple simulations (refer to Appendix B for the details on how we implemented this substitution in the PHANTOM code). The triple obtained by splitting the secondary star can be viewed as a massive body orbited by a lighter binary (*ts* type). If instead the primary is split, the system consists of a massive binary orbited by a third lighter body (*tp* type). The substituting small binary is circular, has a mass ratio $q_{\rm small} = 1$, and has a semimajor axis $a_{\rm small} = 0.1\,a_{\rm wide}$, where $a_{\rm wide}$ is the semimajor axis of the wide binary orbit. The mass of the substituting small binary is equal to the substituted star. With this process, we built up the simulation Set 1, discussed in Section 2.

As shown in Fig. 4, in the parameter space region explored by this simulation set, *ts* and *tp* simulations raise their small binary accretion rate with respect to their single counterpart in the associated binary system. As a consequence, *ts* simulations raise their λ value, while *tp* simulations lower it. In addition, *ts* triples shift λ more than *tp* triples. In Figs 2 and 3, we report the accretion rates and λ factors of every simulation of this work. The binary (solid curve) and the $a_{\rm small} = 1$ au *ts* and *tp* simulations (dashed curves) show how the accretion rates of the single stars contribute in shifting the λ factors. From the single accretion rate data, we see that the small binary always increases its accretion rate, while the tertiary star lowers it. However, the split affects the single star only for lower mass ratios. Indeed, in the $q_{\rm wide} = 0.65$ case, the accretion rate of the single body does not change significantly. This implies that the total accretion rate of the $q = 0.65$ triple systems is not conserved with respect to the binary case. Given that the total accretion rate of the system is set by viscous accretion, it should not be different for different stellar systems surrounded by the same disc. Thus, we conclude that the $q_{\rm wide} = 0.65$ systems have not reached steady state. However, we show in Appendix A that 100 outer binary orbits are enough to measure λ factors in a reliable manner.

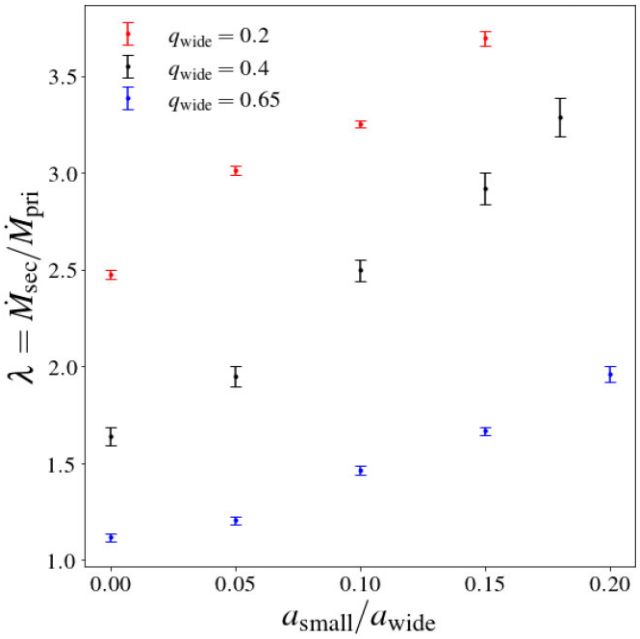

Figure 5. $\lambda = \dot{M}_{\rm sec}/\dot{M}_{\rm pri}$ factors for Set 2 triples. Different colours refer to different mass ratios of the wide orbit $q_{\rm wide}$. $a_{\rm small}/a_{\rm wide} = 0$ points are the associated binary simulations.

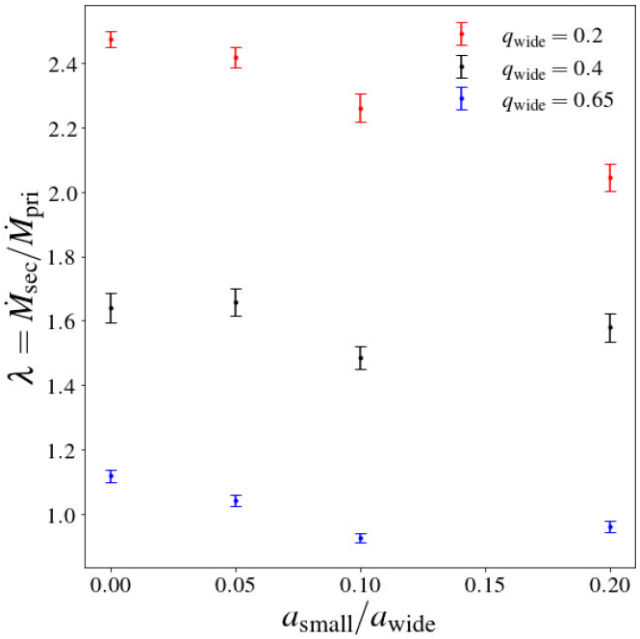

Figure 6. $\lambda = \dot{M}_{\rm sec}/\dot{M}_{\rm pri}$ factors for Set 3 triples. Different colours refer to different mass ratios of the wide orbit $q_{\rm wide}$. $a_{\rm small}/a_{\rm wide} = 0$ points are the associated binary simulations.

3.3 Dependence on $a_{\rm small}$ and prescription for accretion rate deviations in triples

How much accretion rates deviate from the binary case depends on the orbital configuration of the hierarchical triple, in particular on its small binary mass $M_{\rm b}$ and on its small binary semimajor axis $a_{\rm small}$. Indeed, Figs 5 and 6 show how much the triple $\lambda_{\rm t}$ factor deviates from the associated binary $\lambda_{\rm b}$ factor as a function of $a_{\rm small}$ for Set 2

(*ts* type triples, see Section 2) and Set 3 simulations (*tp* type triples, see Section 2), respectively.

The change in the accretion rate of a multiple system star is linked to a variation of the net flux of mass in its Roche lobe. Indeed, in the steady state regime, all the mass that enters the Roche lobe is eventually accreted by the star(s) inside the lobe. This implies that the mechanisms that modify the accretion rate of a body have to act on the scale of its Roche lobe. Two physics phenomena can be invoked in order to describe these deviations: the augmented geometrical cross-section of the small binary and the angular momentum exchange between the small binary and the surrounding gas.

On the one hand, the small binary interacts with the surrounding gas through a geometrical cross-section that is proportional to the area of the small binary orbit A,

$$A \propto a_{\rm small}^2. \tag{15}$$

Thus, we expect that the larger geometrical cross-section of the small binary raises its accretion rate with respect to the corresponding single star in the associated binary system.

On the other hand, we expect the small binary torque on to the surrounding gas to obstruct the accretion of material on to the small binary stars. In the impulse approximation (Lin & Papaloizou 1979), we can estimate the torque exerted by the small binary on to the surrounding gas. If we suppose the small binary mass ratio $q_{\rm small} \ll 1$, the density of tidal torque exerted by the small binary on to a fluid element at a distance p from the secondary star can be approximated by

$$\tau = f q_{\rm small}^2 \Omega_{\rm small}^2 a_{\rm small}^2 \left(\frac{a_{\rm small}}{p}\right)^4, \tag{16}$$

where $\Omega_{\rm small}$ is the small binary frequency and f is a dimensionless normalization factor. Even if this approximation holds for low mass ratio binaries only, it gives us insights about how the specific torque scales with the small binary properties. We can assume that p is approximately equal to the distance between the inner binary stars and the small binary Roche lobe edge; thus, $p \propto R_{\rm Roche}$. Hence, writing explicitly the binary frequency in equation (16), we obtain

$$\tau \propto M_{\rm b} \frac{a_{\rm small}^3}{R_{\rm Roche}^4}, \tag{17}$$

where $M_{\rm b}$ is the small binary mass.

Taking into account the torque scaling and the geometrical cross-section, we propose a parametrization to describe the competition between these mechanisms in modifying the accretion rate of the triple small binary with respect to the corresponding single star in the associated binary system. With this prescription, we also test the relative efficiency of different contributions to the deviations. Deviations are measured by means of the accretion ratio between the accretion rate of the small binary in the triple ($\dot{M}_{\rm t,sec} = \dot{M}_{\rm t,sec1} + \dot{M}_{\rm t,sec2}$) over the accretion rate of the corresponding binary star ($\dot{M}_{\rm b,sec}$). We then fit the accretion ratios with the following prescription:

$$\frac{\dot{M}_{\rm t,sec}}{\dot{M}_{\rm b,sec}} = 1 + \Gamma_\tau \frac{(a_{\rm small}/a_{\rm wide})^3}{(R_{\rm Roche}/a_{\rm wide})^4} + \Gamma_{\rm A} \left(\frac{a_{\rm small}}{a_{\rm wide}}\right)^2, \tag{18}$$

where Γ_τ and $\Gamma_{\rm A}$ are parameters to be fitted and relate to the torque and the geometrical cross-section, respectively. In equation (18), we assume the geometrical term to scale with the small binary cross-section ($\propto a_{\rm small}^2$), and the torque term to scale as in equation (17) ($\propto a_{\rm small}^3/R_{\rm Roche}^4$). We thus expect that for small semimajor axis the cross-section contribution to the accretion rate will dominate the accretion. Meanwhile, for wide semimajor axes, the torque term will be more relevant. In addition, we expect that the torque parameter Γ_τ will be proportional to the small binary mass (as in equation 17), while the geometrical cross-section will depend only on the geometry of the orbits and not on the mass. However, the efficiency of each term depends on Γ_τ and $\Gamma_{\rm A}$.

3.3.1 Secondary split accretion ratios

In order to test the parametrization for the accretion rate deviation due to the splitting, we simulate a second set of hierarchical triples. The aim of this set is to explore different regimes for the accretion ratio varying the semimajor axis of the small binary.

We started from the *ts* triples of Set 1 (with $a_{\rm small} = 1$ au) and we simulated the same *ts* hierarchical triple but with a semimajor axis of the small binary of $a_{\rm small} = 0.5$ and 1.5 au. We also exploited the wider stable range of semimajor axes for high-$q_{\rm wide}$ hierarchical triples (Mardling & Aarseth 2001) in order to simulate even wider small binaries for $q_{\rm wide} = 0.4$ (for which we also simulate $a_{\rm small} = 1.8$ au) and 0.65 systems (with $a_{\rm small} = 2$ au). The accretion rates of this simulation set (called Set 2, see Section 2) are plotted in Fig. 2, and their average $\lambda_{\rm t}$ factors are reported in Fig. 5.

In order to apply the prescription in equation (18), we compute the ratio between the accretion rate of the small binary ($\dot{M}_{\rm t,sec}$) over the accretion rate of the secondary star in the associated binary system ($\dot{M}_{\rm b,sec}$). When the repulsing effect of the binary torque contributes more than the geometrical cross-section to the accretion rate deviation, we expect this accretion ratio to be less than 1. On the contrary, when the cross-section dominates, the ratio will be larger than 1. Fig. 7 shows $\dot{M}_{\rm t,sec}/\dot{M}_{\rm b,sec}$ varying the small binary semimajor axis.

Widening the inner binary, each $q_{\rm wide}$ data set in Fig. 7 follows a similar trend: a steep raise for smaller small binary semimajor axes, followed by lower deviations for larger small binary semimajor axes. Accretion ratios clearly depend on $q_{\rm wide}$, which in turn depends on the small binary mass. Indeed, for a given small binary semimajor axis, more massive small binaries systematically correspond to higher deviations in the accretion rate. Thus, the extent of the deviation depends on the split star mass. In the explored semimajor axis range, the accretion ratios are always higher than unity. Thus, the geometrical cross-section contribution to the deviation is greater than the torque contribution in each triple we considered.

In order to study how Γ_τ and $\Gamma_{\rm A}$ depend on the small binary mass, we separately fit the data point of each mass ratio (i.e. the blue, black, and red points in Fig. 7) with the prescription in equation (18). We thus obtain for each mass ratio the values of Γ_τ and $\Gamma_{\rm A}$ that best fit our data. These values are plotted in Fig. 8. The parameter Γ_τ scales linearly with the small binary mass $M_{\rm b}$, as expected from equation (17). Also, $\Gamma_{\rm A}$ depends on the small binary mass, in contrast with what we expect from a purely geometric cross-section. The dependence of $\Gamma_{\rm A}$ on $M_{\rm b}$ can be due to a gravitational focusing effect. Indeed, without gravitational focusing, gas with an impact parameter higher than $a_{\rm small}$ skips the small binary geometric cross-section. On the contrary, in the gravitationally focused limit, gas with an impact parameter higher than $a_{\rm small}$ can enter the cross-section of the small binary. This is because the relative velocity between the gas and the binary is lower than the escape velocity from it. In this limit, more massive binaries have a larger effective cross-section, as noticed in the plot.

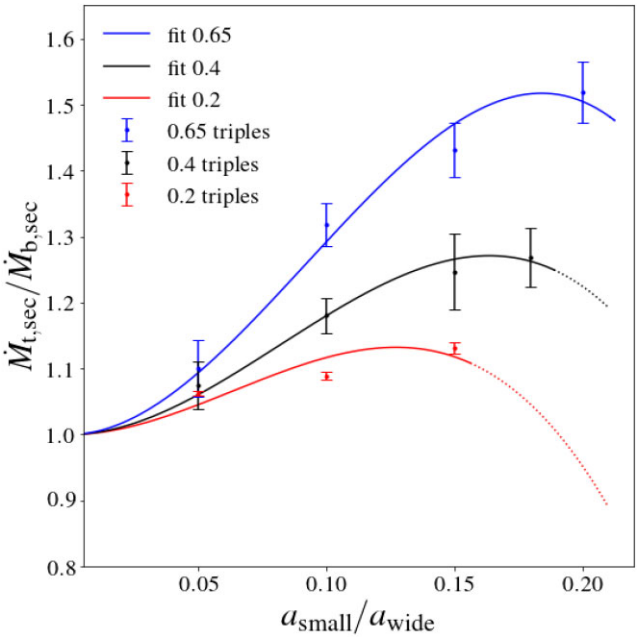

Figure 7. Set 2 deviations in the small binary accretion rate as a function of the small binary semimajor axis. These simulations are obtained by splitting the secondary star of the three binaries of Set 1. The dots are the ratios between the accretion rate of the small binary ($\dot{M}_{\rm t,sec}$) and the accretion rate of the secondary star in the associated binary system ($\dot{M}_{\rm b,sec}$). The curves are obtained by fitting the three parameters of our prescription (equation 18) for each mass ratio of the wide orbit (0.2, 0.4, and 0.65 for red, black, and blue curves, respectively). The dotted part of each curve denotes the semimajor axis range for which the hierarchical triples are unstable.

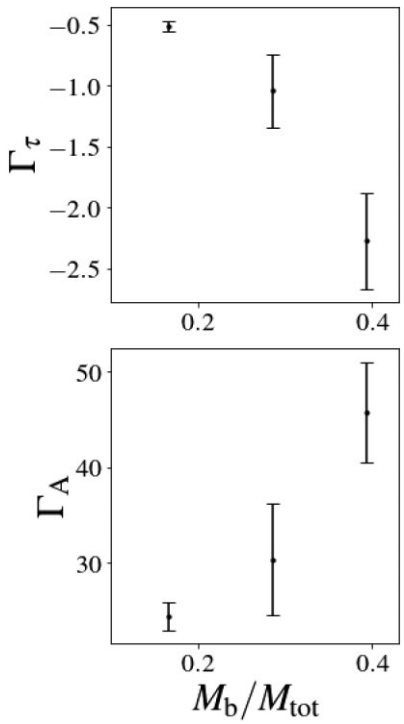

Figure 8. Best-fitting Γ parameters for our prescription (equation 18) as a function of the small binary mass. $M_{\rm b}$ and $M_{\rm tot}$ are the mass of the inner binary and of the system, respectively.

3.3.2 *Primary split accretion ratios*

We study how the accretion rate varies as a function of the orbital parameters of the triple when splitting the primary star. Primary and secondary stars are expected to accrete gas from the disc inner edge in different ways. On the one hand, the secondary has access to the gas stored in the disc mainly by pulling streamers directly from the inner edge. These streamers fill the secondary star Roche lobe (and to a lesser extent the cavity) with gas, allowing gas to fall on to the secondary star. On the other hand, the primary star pulls less massive streamers than the secondary, particularly for low mass ratios. Thus, the primary provides less gas directly from the disc, resulting in lower accretion rates. Another viable way for gas to reach the primary star is by means of the L1 point between the Roche lobes of the two binary stars. The more gas crosses the L1 point towards the primary, the higher its accretion rate at the expense of the secondary star. As said, in hotter discs, the accretion rates of the two stars are more even also thanks to this gas exchange (Young et al. 2015).

Raising the mass ratio $q_{\rm wide}$, these differences level out and the primary becomes more and more independent from the secondary in filling its Roche lobe with gas. As a result, the closer $q_{\rm wide}$ is to unity, the more the primary and secondary stars accrete mass in a similar way. On the contrary, away from $q_{\rm wide} = 1$, we expect the primary to be in a gas-poor environment, which prevents it from efficiently accreting mass. We expect these differences to result in different differential accretion deviations when splitting the primary star, rather than the secondary. Indeed, the split of the primary can either raise the mass that crosses L1 or raise the mass that falls on to the small binary from the inner edge. Thus, we tested the primary split configurations in Set 3.

In Set 3, we simulate a set of *tp* hierarchical triples, based on the *tp* simulations of Set 1 (with $a_{\rm small} = 1$ au), varying the small binary semimajor axis ($a_{\rm small} = 0.5$, 2 au, see Section 2). Fig. 3 shows the accretion rates of Set 3 simulations, and Fig. 6 shows their average $\lambda_{\rm t}$ factors.

The greater λ factor deviations are observed in the $q_{\rm wide} = 0.2$ systems (Fig. 6). The deviations are due to an enhanced flow through the L1 point; indeed, as shown in Fig. 3, the raise in the accretion rate of the small binary is at the expense of the accretion rate of the third body. Fig. 6 also shows that wider small binaries more easily capture mass from the third body Roche lobe, further reducing their λ factor.

Hierarchical triples with $q_{\rm wide} = 0.4$ and 0.65 show smaller or no deviations due to the splitting. Indeed, in Fig. 2, their λ factors reduce up to 0.9 times the binary λ factor. Thus, for higher mass ratios of the outer orbit, the small binary is less efficient in stealing mass from the third body Roche lobe. In addition, and contrary to the $q_{\rm wide} = 0.2$ case, wider small binary semimajor axes affect the deviations in λ only modestly, as the impact of the geometrical cross-section is limited by the availability of mass in the surrounding of the small binary.

In light of this, the deviation observed in triples obtained by splitting the primary star cannot be captured by the effects described in equation (18). In Fig. 9, we show the ratios between the accretion rate of the small binary over the accretion rate of its single counterpart in the associated binary system. Only for high $q_{\rm wide}$, we recover the trend observed in Fig. 7, as the small binary starts to accrete more similarly to the secondary star of a binary, for which equation (18) holds.

It is important to notice that the accretion rates of primaries and *tp* triple small binaries are not fully resolved (as discussed in Appendix A). Thus, the numerical results of this section have to be

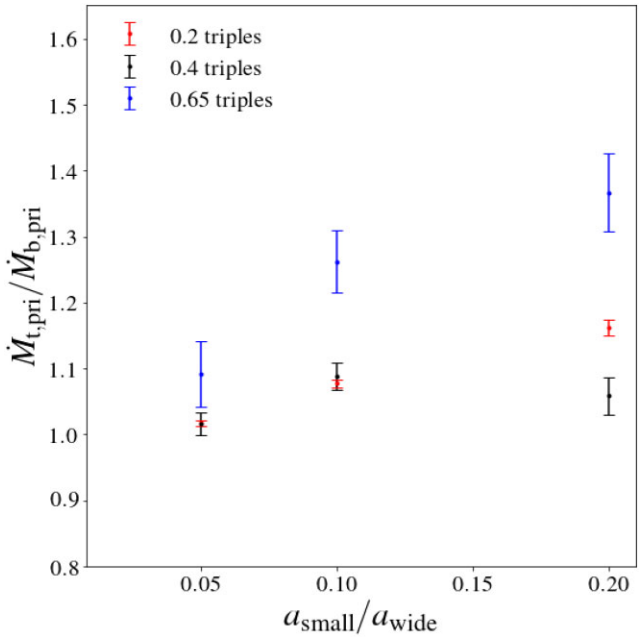

Figure 9. Set 3 deviations in the small binary accretion rate as a function of the small binary semimajor axis. These simulations are obtained by splitting the primary star of the three binaries of Set 1. The dots are the ratios between the accretion rate of the small binary ($\dot{M}_{t,pri} = \dot{M}_{t,pri1} + \dot{M}_{t,pri2}$) and the accretion rate of the primary star in the associated binary system ($\dot{M}_{b,pri}$).

treated with caution. These results are still relevant as we report the *relative* deviations due to the splitting measured for different choices of orbital parameters and we never rely on the absolute values that we measure in our simulations.

4 ACCRETION IN HIERARCHICAL TRIPLE SYSTEMS

4.1 Deviations of triple differential accretion from the associated binary system

We have shown that hierarchical triples embedded in accretion discs have a peculiar way to distribute disc mass between the stars of the system. The ground state of differential accretion in hierarchical triples is based on the binary dynamics. Indeed, to a first approximation, the wide orbit of the hierarchical triple mimics a binary system and it accretes mass in the same way, favouring the lighter body of the system. However, at smaller scales, the influence of the triple system small binary has to be taken into account. The small binary–gas interaction changes the accretion rates of the three stars in relative terms (changing the proportion in which mass distributes among the stars, as shown in Fig. 4). Having a larger geometrical cross-section, the small binary increases its accretion rate. This geometrical mechanism competes with the tendency of the small binary gravitational torque to repel the surrounding gas out of its Roche lobe. This competition gives the peculiar shape of the deviations in the accretion rate of the small binary as a function of its semimajor axis, as shown in Figs 7 and 8.

This mechanism generally shifts the triple system λ_t factor in favour of the small binary. However, how much λ_t deviates from the associated binary λ_b factor depends also on the mass ratio of the triple system wide orbit (q_{wide}). Indeed, lower mass ratios show higher deviations from the associated binary, both when the small binary is lighter and heavier than the third body. Moreover, the triples obtained by splitting the secondary star of a binary result in higher deviations, compared to triples obtained by splitting the primary star (see Section 3.3.2).

4.2 Differential accretion in hierarchical triples

The main consequence of differential accretion in binary systems is a tendency to equalize system masses. Indeed, as discussed in previous works (Farris et al. 2014; Kelley et al. 2019; Duffell et al. 2020), with enough mass at disposal, the higher accretion rate of the secondary star pushes the mass ratio of the system towards unity.

In this work, we found that a hierarchical triple system in which the small binary is lighter than the third body raises the wide binary mass ratio q_{wide} more effectively than its associated binary system. Indeed, in the parameter space explored, the hierarchical triple λ_t factor (defined in equation 11) is higher than the λ_b factor of its associated binary (defined in equation 9).

For a quantitative comparison, the $q_{wide} = 0.65$ configuration (the one with the lowest λ_t among Set 1) has $\lambda_t \approx 1.3\lambda_b$, when splitting the secondary star of the associated binary. Even if we account only for the mass equalization due to the triple mechanism (i.e. if we consider $\lambda_b = 1$), we found that the small binary accretion rate is 1.3 times higher than the primary one. The binary differential accretion mechanism alone allows us to obtain such a disequilibrium in the accretion rates only for q_B lower than 0.35 or 0.75 for K19 and D20 parametrizations (respectively), as shown in Fig. 4. For wider small binary semimajor axes or lower wide orbit mass ratios, the triple differential accretion mechanism is even more efficient. In addition, the disequilibrium between the stellar accretion rates in triples is at play even if $q_{wide} \approx 1$, where binary differential accretion is turned off.

We also remind that binary prescriptions strongly depend on the circumbinary gas properties and we do not know how they behave in actual protostellar disc conditions. On the contrary, we showed that the larger than unity λ_t/λ_b ratio is due to the increased cross-section of the small binary, which solely depends on the geometry of the orbits. Thus, we expect this ratio to be independent of the disc conditions. This difference is important because Duffell et al. (2020) showed that binary differential accretion is turned off in low-viscosity regimes, where they found $\lambda \approx 1$ independently of the mass ratio. If this result is confirmed, we expect binary differential accretion to be turned off for low-viscosity protostellar discs. But, if the larger than unity λ_t/λ_b ratio is preserved (as we expect), the differential accretion in hierarchical triples constitutes the only viable mechanism to equalize the stellar masses.

Assuming $\lambda_b = 1$, as in protostellar disc condition independently of q (Duffell et al. 2020) or as in more viscous discs around high-q systems, we can explicitly study the evolution of q with time in the binary and in the hierarchical triple case. Under the approximation of a constant accretion rate (e.g. due to an infall that replenishes the outer part of the disc), we obtain the following differential equation for q:

$$\frac{\mathrm{d}q}{\mathrm{d}t_{acc}} = \frac{q+1}{\lambda(q)+1}\left(\lambda(q) - q\right), \tag{19}$$

where $t_{acc} = (\dot{M}_{tot}/M_{tot})t$ is the time in units of the mass doubling time of the system, with $\dot{M}_{tot}$ and M_{tot} the total system accretion rate and mass, respectively. Solving equation (19), we obtain the times needed by a hierarchical triple and by a binary (τ_t and τ_b, respectively) in order to reach a given wide orbit mass ratio q_{wide} starting from the same initial mass ratios q_0. Fig. 10 shows τ_t/τ_b as a function of the final wide orbit mass ratio q_{wide} for three

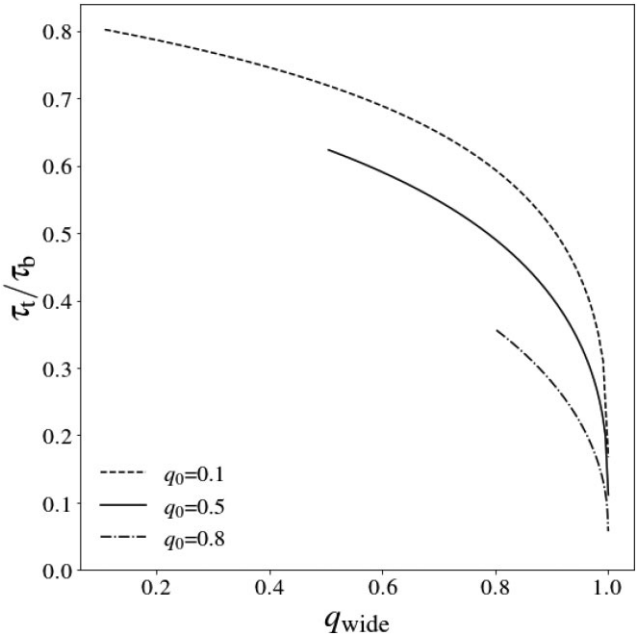

Figure 10. Ratio of the times needed in order to reach a certain q_{wide} by a triple (τ_t) and by a binary (τ_b). Different curves refer to different initial mass ratios q_0. Curves are obtained by solving equation (19) with $\lambda(q_{wide}) = 1$ for binaries and $\lambda(q_{wide}) = 1.3$ for triples.

different initial mass ratios q_0. We assume $\lambda(q_{wide}) = 1$ for binaries and $\lambda(q_{wide}) = 1.3$ for triples, that is the triple λ factor we expect from the λ_t/λ_b ratio measured in our simulations, as discussed in the previous paragraphs. The equalizing time for hierarchical triples (i.e. the time needed to reach $\lambda(q_{wide}) = 1$) is nearly an order of magnitude lower than the binary equalizing time, in particular for high-q_{wide} systems.

A more subtle difference between the two mechanisms is the final equilibrium point of the wide orbit mass ratio q_{wide}. Indeed, from equation (19), we see that the equilibrium point for q_{wide} is at $q_{wide} = \lambda$. Thus, because (i) binary differential accretion prescriptions tend to unity for increasing q_{wide} and (ii) symmetry reasons suggest that an equal-mass binary has $\lambda_b = 1$, we expect binaries to stall at a mass ratio $q_{wide} = 1$. Conversely, for a triple with a small binary heavier than the single body, we expect a λ_t lower than unity due to the raise in the small binary accretion rate. Thus, hierarchical triple systems stall at a mass ratio q_{wide} smaller than unity as well. The extent of this equilibrium shift depends on the specific orbital parameters of the system, which are responsible for the shift in λ_t. This work suggests an equilibrium point for triple systems of $q_{wide} \approx 0.9$. Indeed, λ_t/λ_b measured in our triple systems with small binary heavier than the single star is approximately 0.9. Thus, we expect that around $q_{wide} = 1$, where $\lambda_b \approx 1$ as well, $\lambda_t = 0.9$.

4.3 Multiplicity signatures in differential accretion

In principle, with perfect knowledge of binary differential accretion and of its dependence on the binary mass ratio q_{wide}, the gas viscosity, and temperature, we could be able to infer from an observed λ_b in a binary system the presence of an unresolved small binary. Indeed, in case of binary accretion rates not in line with the binary theory, we could invert the relation proposed in equation (18) in order to obtain the a_{small} of a possible unresolved small binary. However, up to now, binary prescriptions do not take into account dependences other than q_{wide}.[2]

In addition, the disc conditions explored in this work (and in the main works on this topic in the literature) are halfway between the compact object accretion discs (that are thinner than the aspect ratio used) and protoplanetary discs (that are orders of magnitude less viscous), and thus do not represent either case. Moreover, we limited our investigation to: (i) circular wide and small binary orbits, (ii) equal-mass small binaries, and (iii) coplanar configurations. This allowed us to simplify the problem and observe the specific signatures of the geometrical and torque effects described in this work.

We expect the mechanism proposed in this work to be at play in more complex configurations as well. However, its efficiency will be surely affected. This is mainly due to the dependence of both the accretion rate and the small binary torque on the orbital parameters of a given multiple system. In particular, the eccentricity and the mutual inclinations between the orbital planes and the discs are likely to play a major role since they can induce tilt oscillations and precession, which would translate into phase-dependent accretion rates along the orbit. A known example of a system where a highly eccentric binary shows phase-modulated accretion rates is discussed in Dunhill et al. (2015), where they show that for a limited amount of time it is possible for the primary to accrete more mass than the secondary.

Given these limitations, the only remaining case that at the moment could highlight an unresolved small binary in an accreting binary system is a system where $\lambda < 1$ is observed. In that case, no binary configuration can reproduce this behaviour (except with a high eccentricity) and the only explanation that can be addressed to solve the puzzle should be a massive unresolved small binary, whose geometrical cross-section counterbalances the tendency of binary differential accretion to favour the secondary single star. However, in our simulations, even such configurations hardly push under 1 the ratio between the accretion rates, as can be seen in Fig. 3 and discussed in Section 3.3.2. Although in principle this should be possible for mass ratios greater than the ones explored in this work, the parameter space region where significant signatures of a hidden small binary could appear remains small.

Thus, the goal to exploit the deviation of the observed λ_t in a triple system from the λ_b expected in its associated binary system is complicated by these additional dependences and at the moment we cannot disentangle deviations due to different mechanisms, which change λ without the need to invoke a higher multiplicity.

5 CONCLUSIONS

In this work, we presented hydrodynamical simulations of discs in hierarchical triple systems. We focus on the accretion process from the circumtriple disc on to the individual stars of the system. In particular, we studied how the presence of the small binary affects the accretion rates of the individual stars.

We performed a set of simulations in order to span different hierarchical triple system configurations using the SPH code PHANTOM. We proposed a semi-analytical prescription (given by equation 18) that is able to describe the data we obtained in our simulations.

Our main findings are the following:

(i) Differential accretion in hierarchical triple systems can be explained by the interplay between two contrasting mechanisms: (1) the increased geometrical cross-section between gas and small

[2]Although in Young & Clarke (2015) a trend related to temperature is suggested, further studies are needed to constrain an effective parametrization.

binary, and (2) its angular momentum exchange with it. These two mechanisms are superimposed on the binary differential accretion process.

(ii) The small binary torque is too weak to counterbalance the increased accretion rate of the small binary due to the larger cross-section, except for very wide small binary semimajor axes ($a_{\rm small}$) that result in unstable hierarchical triples. Thus, in the vast majority of the stable hierarchical triple parameter space, the small binary accretes more mass than if it would be a single star of the same mass. As a result, if the hierarchical triple small binary is heavier than the third body, the standard differential accretion scenario (whereby the secondary accretes more of the mass) is hampered. Reciprocally, if the small binary is lighter than the third body, the standard differential accretion scenario is enhanced.

(iii) Hierarchical triple systems with a small binary lighter than the single star equalize their masses nearly an order of magnitude quicker than binary systems. Conversely, in triples with a small binary heavier than the single star, mass equalization is slowed down. In contrast with binaries, the equilibrium mass ratio for triple systems is lower than 1.

In conclusion, the mass ratio in accreting hierarchical triple stellar systems evolves differently compared to binaries. These differences, during the disc lifetime, are expected to produce characteristic mass ratio distributions, which could possibly be observed through ongoing and future surveys. Further observational data will help to test and further constrain the proposed accretion model for triple stellar systems. At any rate, the orbital parameters and initial masses play a crucial role in determining the final stellar mass ratios in high-order multiple stellar systems.

ACKNOWLEDGEMENTS

The authors thank the referee for their constructive feedback and suggestions, which have significantly improved the original manuscript. This project has received funding from the European Union's Horizon 2020 research and innovation programme under the Marie Skłodowska-Curie grant agreement nos 210021 and 823823 (DUST-BUSTERS). SC thanks Cristiano Longarini and Pietro Curone for useful discussions. This work used SPLASH (Price 2007) for SPH data visualization. The authors used the following PYTHON tools and packages: NUMPY (Harris et al. 2020), MATPLOTLIB (Hunter 2007), and JUPYTER (Kluyver et al. 2016).

DATA AVAILABILITY

The data underlying this paper will be shared on reasonable request to the corresponding author. The code PHANTOM used in this work is publicly available at https://github.com/danieljprice/phantom.

REFERENCES

Alves F. O., Caselli P., Girart J. M., Segura-Cox D., Franco G. A. P., Schmiedeke A., Zhao B., 2019, Science, 366, 90
Artymowicz P., Lubow S. H., 1996, ApJ, 467, L77
Bate M. R., 2000, MNRAS, 314, 33
Bate M. R., 2009, MNRAS, 397, 232
Bate M. R., 2018, MNRAS, 475, 5618
Bate M. R., Bonnell I. A., 1997, MNRAS, 285, 33
Bate M. R., Bonnell I. A., Price N. M., 1995, MNRAS, 277, 362
Bi J. et al., 2020, ApJ, 895, L18
Binnendijk L., 1960, Properties of Double Stars: A Survey of Parallaxes and Orbits. Univ. Pennsylvania Press, Philadelphia, PA
Bonnell I. A., Bate M. R., 1994, MNRAS, 271, 999
Chen X. et al., 2013, ApJ, 768, 110
Connelley M. S., Reipurth B., Tokunaga A. T., 2008, AJ, 135, 2526
Di Folco E. et al., 2014, A&A, 565, L2
Duchêne G., Kraus A., 2013, ARA&A, 51, 269
Duffell P. C., D'Orazio D., Derdzinski A., Haiman Z., MacFadyen A., Rosen A. L., Zrake J., 2020, ApJ, 901, 25
Dullemond C. P. et al., 2018, ApJ, 869, L46
Dunhill A. C., Cuadra J., Dougados C., 2015, MNRAS, 448, 3545
Duquennoy A., Mayor M., 1991, A&A, 500, 337
Eggleton P. P., 1983, ApJ, 268, 368
Farris B. D., Duffell P., MacFadyen A. I., Haiman Z., 2014, ApJ, 783, 134
Gerosa D., Veronesi B., Lodato G., Rosotti G., 2015, MNRAS, 451, 3941
Gingold R. A., Monaghan J. J., 1977, MNRAS, 181, 375
Goldreich P., Tremaine S., 1980, ApJ, 241, 425
Harris C. R. et al., 2020, Nature, 585, 357
Hartmann L., Calvet N., Gullbring E., D'Alessio P., 1998, ApJ, 495, 385
Hunter J. D., 2007, Comput. Sci. Eng., 9, 90
Kelley L. Z., Haiman Z., Sesana A., Hernquist L., 2019, MNRAS, 485, 1579
Keppler M. et al., 2020, A&A, 639, A62
Kluyver T. et al., 2016, in Loizides F., Schmidt B., eds, Positioning and Power in Academic Publishing: Players, Agents and Agendas. Jupyter Notebooks – a publishing format for reproducible computational workflows, IOS Press, p. 87
Kraus S. et al., 2020, Science, 369, 1233
Lin D. N. C., Papaloizou J., 1979, MNRAS, 186, 799
Lodato G., Price D. J., 2010, MNRAS, 405, 1212
Lucy L. B., 1977, AJ, 82, 1013
Lynden-Bell D., Pringle J. E., 1974, MNRAS, 168, 603
Mardling R. A., Aarseth S. J., 2001, MNRAS, 321, 398
Muñoz D. J., Lai D., 2016, ApJ, 827, 43
Muñoz D. J., Lai D., Kratter K., Miranda R., 2020, ApJ, 889, 114
Phuong N. T. et al., 2020, A&A, 635, A12
Price D. J., 2007, PASA, 24, 159
Price D. J. et al., 2018, PASA, 35, e031
Ragusa E., Lodato G., Price D. J., 2016, MNRAS, 460, 1243
Reipurth B., Clarke C. J., Boss A. P., Goodwin S. P., Rodríguez L. F., Stassun K. G., Tokovinin A., Zinnecker H., 2014, in Beuther H., Klessen R. S., Dullemond C. P., Henning T., eds, Protostars and Planets VI. Univ. Arizona Press, Tucson, p. 267
Reynolds N. K. et al., 2021, ApJ, 907, L10
Shakura N. I., Sunyaev R. A., 1973, in Bradt H., Giacconi R., eds, Proc. IAU Symp. 55, X- and Gamma-Ray Astronomy. Reidel, Dordrecht, p. 155
Tobin J. J. et al., 2016, ApJ, 818, 73
Valtonen M., Karttunen H., 2006, The Three-Body Problem. Cambridge Univ. Press, Cambridge
Young M. D., Clarke C. J., 2015, MNRAS, 452, 3085
Young M. D., Baird J. T., Clarke C. J., 2015, MNRAS, 447, 2907

APPENDIX A: NUMERICAL TESTS

A1 Accretion rate dependence on accretion prescription and spatial resolution

The accretion rate on to the stars of each stellar system is the main observable measured in this work. In the following sections, we detail the numerical tests we performed to check that the measured accretion rates are reliable. In the first section, we discuss how the accretion rates depend on the accretion prescription we used in our simulations. In the second section, we test if the measured accretion rates are fully resolved in our numerical simulations.

A1.1 Accretion prescription

Given that we used sink particles, there is only one possible numerical choice when setting the simulation: the sink radius $R_{\rm sink}$. SPH particles inside a sphere of radius 0.8 $R_{\rm sink}$ are automatically accreted on to the sink. The other particles inside a sphere of radius $R_{\rm sink}$ are accreted only if they are both gravitationally bound to the sink and have a sufficiently low angular momentum (Bate et al. 1995; Price et al. 2018). In all our simulations, we set all the accretion radii equal to 0.1 au. This radius is roughly 4 per cent of the smallest Roche lobe radius around secondary stars in binaries (i.e. the smallest Roche lobe radius around small binaries in triples).

To test how the choice of sink radii affects stellar accretion, we ran two additional simulations doubling and halving all sink radii of our reference simulation (the *ts*2 triple in Set 1). We integrated these two configurations for 100 outer orbit periods and we compared the accretion rates with the reference simulation.

Fig. A1 shows the accretion rates and λ factors of test simulations, along with the reference one. We found that deviations from the reference simulation due to different sink radii are lower than 2 per cent. The deviations due to the splitting we measure in this work are at least one order of magnitude higher, particularly in triples with the small binary lighter than the third body (compare Fig. A1 with Fig. 2). Since the accretion rates are not affected by the choice of the accretion radius, we conclude that our sink particles measure stellar accretion properly.

A1.2 Spatial resolution

To model accretion on to the stars in a realistic way, we simulate the entire circumtriple disc. This choice limits our ability to carefully model the formation and evolution of circumstellar discs. The simulations presented in this paper barely resolve inner discs in the cavity of the circumtriple disc. These discs do form within the cavity but with a limited spatial resolution. Indeed, the spatial resolution in the immediate surrounding of the stars is about 20 per cent of the Roche lobe radius (i.e. the spatial scale of the expected circumstellar discs).

The net flux of mass through the Roche lobe boundary around each star is the quantity that sets the individual accretion rates. The formation of discs inside the Roche lobes can introduce a delay during the disc formation phase. However, the mass that enters a given lobe will eventually fall on to the star. Indeed, mass cannot accumulate indefinitely in the Roche lobe. Here, we wish to investigate whether the numerical resolution is high enough to ensure that the accretion rates on to the stars are well resolved.

To test the resolution of our simulations, we ran two additional simulations: We multiplied by 4 and divided by 2 the number of particles in the *ts*2 reference simulation, obtaining a higher resolution simulation of 4 million particles and a lower resolution simulation with 500k particles. We ran the higher resolution simulation for 40 outer orbit periods and the lower resolution simulation for 100 orbits. Their accretion rates and λ factors are shown in Fig. A2.

The simulations show that the accretion rate of secondaries is fully resolved: The simulations at higher and lower resolution exhibit the same accretion rates as the reference simulation. We note that the accretion rate of the primary grows with resolution. This implies that the circumprimary disc material is not fully resolved. Hence, we conclude that our results based on secondary splitting and the resulting accretion rate deviations are not affected by resolution issues. However, the measured λ factors (both in binaries and in triples) are slightly overestimated, due to the underestimation of the primary accretion rate. The configuration we tested is the most affected by this issue, as it is the one with the lower primary accretion rate. Here, the λ factor is overestimated by ≈ 8 per cent. It is worth highlighting that the ratio of λ factors constitutes a more reliable quantity given that we are comparing binary and triple simulations *at the same resolution*. However, our results about primary splitting (Section 3.3.2) have to be dealt with more caution. Our results are still relevant in the sense that – instead of discussing individual accretion rates – we report the relative deviations measured for different choices of orbital parameters.

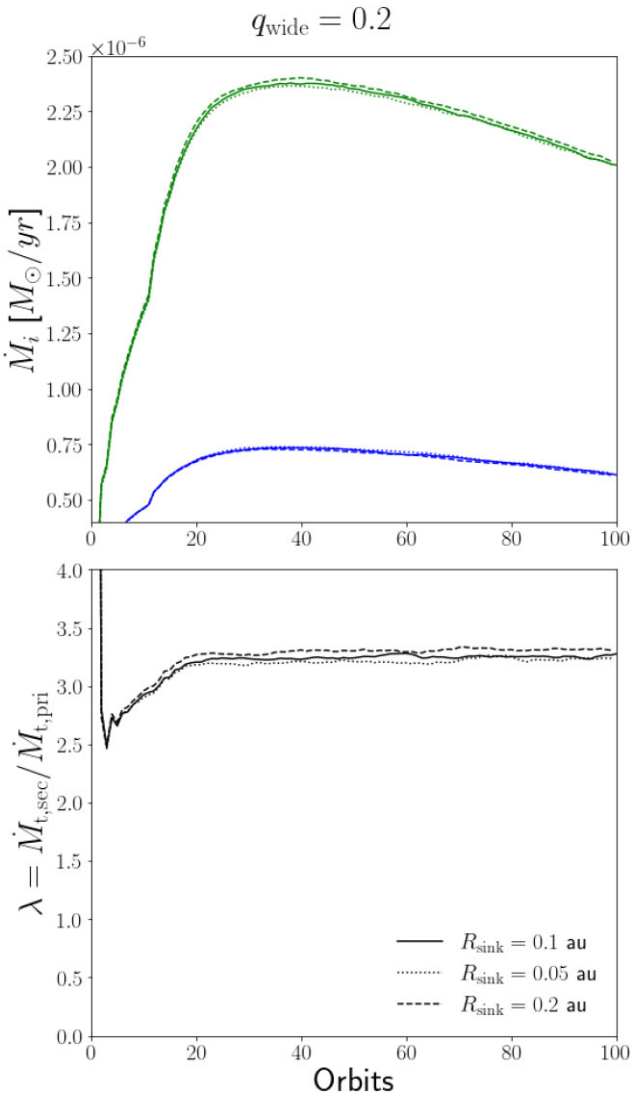

Figure A1. Accretion rates and $\lambda = (\dot{M}_{\rm t,sec1} + \dot{M}_{\rm t,sec2})/\dot{M}_{\rm t,pri}$ factors measured in the triple simulations run to test the accretion prescription. In the upper panel are plotted the accretion rates of the secondary (green) and primary (blue) star. In the lower panel is plotted the ratio between the accretion rates. The solid line refers to the reference simulation *ts*2. Different line styles refer to different sink radii. The secondary accretion rate for the triple system is the sum of the accretion rates of the small binary stars.

A2 Integration time

Our simulations in Sets 1, 2, and 3 last 100 outer orbit periods. As discussed in Section 2, this time span is half a viscous timescale at the inner edge of the disc. Thus, by the end of the

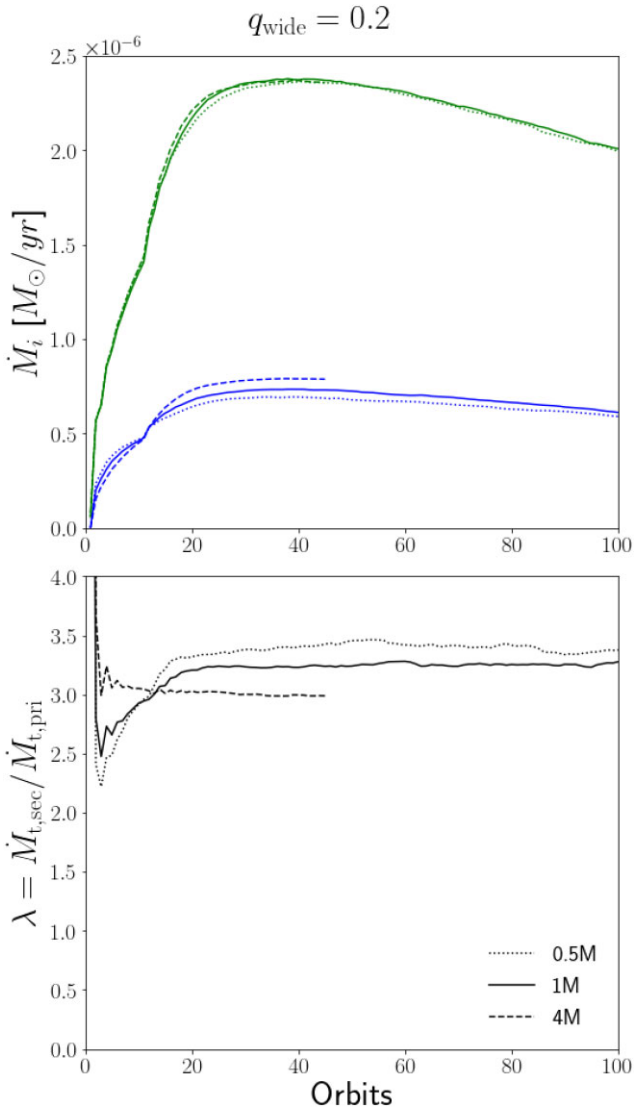

Figure A2. Accretion rates and $\lambda = (\dot{M}_{\rm t,sec1} + \dot{M}_{\rm t,sec2})/\dot{M}_{\rm t,pri}$ factors measured in the triple simulations run to test the resolution. In the upper panel are plotted the accretion rates of the secondary (green) and primary (blue) star. In the lower panel is plotted the ratio between the accretion rates. The solid line refers to the reference simulation *ts*2. Dotted and dashed lines refer to the lower and higher resolution simulations, respectively. The secondary accretion rate for the triple system is the sum of the accretion rates of the small binary stars.

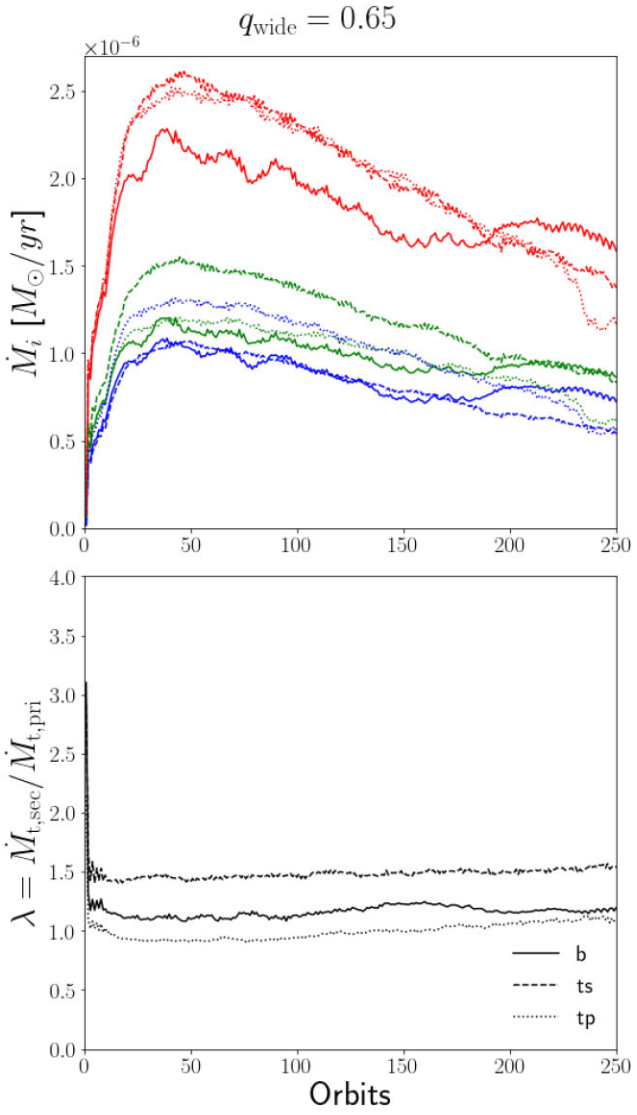

Figure A3. Accretion rates and $\lambda = (\dot{M}_{\rm t,sec1} + \dot{M}_{\rm t,sec2})/\dot{M}_{\rm t,pri}$ factors measured in the triple simulations run to test longer integration times. In the upper panel are plotted the total accretion rate of the system (red) and the accretion rate of the secondary (green) and primary (blue) star. In the lower panel is plotted the ratio between the accretion rates (secondary over primary). The solid, dashed, and dotted lines refer to the binary (*b*65), *ts* triple (*ts*65), and *tp* triple (*tp*65) simulations, respectively. The secondary (primary) accretion rate for the *ts* (*tp*) triple system is the sum of the accretion rates of the small binary stars.

simulation, the circumtriple disc has not reached steady state. Given the number of simulations required to perform the analysis made in this work, modelling the entire disc viscous evolution is beyond our computational ability. Moreover, note that the configuration considered here, where the mass reservoir in the evolving disc is limited, will not actually settle into a steady state even for longer times. However, in this work, we are interested in the way in which mass distributes from the circum-multiple disc over the stellar system stars. This is well measured by the ratio of the stellar accretion rate. In all the simulations we run, these ratios show an initial transient of less than 20 binary orbits – regardless of the multiplicity and of the orbital parameters of the system, before settling down into quasi-equilibrium. To further test this, we ran the three $q_{\rm wide} = 0.65$ simulations in Set 1 for longer integration times. Fig. A3 shows the accretion rates and the λ factors measured in these simulations. We find that, independently of the total accretion rate, mass divides between the sinks in the same way (i.e. we measure a constant λ factor) until the gas smoothing length in the surrounding of the small binary exceeds the small binary semimajor axis. This happens around 250 orbits, and it is a purely numerical effect caused by the loss of resolution around the small binary. Thus, even if the total accretion rate will evolve towards the steady state, we expect the accretion rate ratios to remain constant. This allowed us to reliably measure the λ factors even if our simulations have not reached a steady state.

APPENDIX B: SETTING UP HIERARCHICAL TRIPLE SYSTEMS WITH PHANTOM

The orbital arrangements of observed triple systems tend to be hierarchical, as different configurations are often unstable and have shorter lifetimes. A hierarchical triple (hereafter HT) system consists of a binary (m_1 and m_2) and a distant star (m_3) that orbits the centre of mass of the inner binary. If the third body is sufficiently distant, an analytical perturbative approach is possible in order to compute the evolution of the system. In that case, a first approximation of the inner and the outer orbit is the exact two-body orbit. Indeed, at each instant, we can neglect the perturbations due to the *triplicity* of the system and compute the orbital elements of the elliptical orbits that the three bodies would follow. These elements are called osculating elements. The set regarding the inner binary describes the orbit that the inner bodies would follow if the third body would instantaneously disappear. The set referring to the third body describes the orbit that it would follow if the inner binary was reduced to a single body with the total mass of the binary and in its centre of mass.

In the case of an HT system, we can thus describe the instantaneous state of the system again with 10 elements: the binary mass ratio $q = m_2/m_1$, the triple mass ratio $Q = m_3/(m_1 + m_2)$, the semimajor axis ratio, the two eccentricities, the two initial anomalies, and the three Eulerian angles to orient the orbits in respect to each other.

In order to simulate the stellar system configurations discussed in this work, we implemented in PHANTOM the possibility to set as initial condition an HT system embedded in a Keplerian circumtriple disc. Even if this work focused on a coplanar orbit only, PHANTOM is also able to set a misaligned HT configuration. For future reference, we briefly describe the way in which HTs are initialized in the code.

The initial position and velocity of the two binary bodies are computed by means of the Thiele–Innes elements (Binnendijk 1960). Thiele–Innes elements are computed in terms of the Campbell elements through the following relations:

$$\begin{aligned}\boldsymbol{P} = (&\cos\omega\cos\Omega - \sin\omega\cos i\sin\Omega,\\ &\cos\omega\sin\Omega + \sin\omega\cos i\cos\Omega,\\ &\sin\omega\sin i),\end{aligned} \tag{B1}$$

$$\begin{aligned}\boldsymbol{Q} = (&-\sin\omega\cos\Omega - \cos\omega\cos i\sin\Omega,\\ &-\sin\omega\sin\Omega + \cos\omega\cos i\cos\Omega,\\ &\cos\omega\sin i),\end{aligned} \tag{B2}$$

$$A = \cos E - e, \tag{B3}$$

$$B = \sqrt{1-e^2}\sin E, \tag{B4}$$

where ω, Ω, i, a, and e are the argument of the pericentre, the argument of the ascending node, the inclination, the semimajor axis, and the eccentricity of the binary orbit, respectively, and E is the eccentric anomaly. With equations (B1)–(B4), we can compute the rectangular coordinates and velocities of a given initial condition as

$$(x, y, z) = a(A\boldsymbol{P} + B\boldsymbol{Q}), \tag{B5}$$

$$(v_x, v_y, v_z) = -a\dot{E}(\sin E\boldsymbol{P} - \sqrt{1-e^2}\cos E\boldsymbol{Q}), \tag{B6}$$

where $\dot{E}$ is the time derivative of the eccentric anomaly. The eccentric anomaly E and its derivative $\dot{E}$ are computed from the true anomaly of the orbit.

The HT system initial condition is built by means of the osculating elements of the outer and of the inner binary orbit. First, the code builds a binary with the orbital parameters of the outer orbit. Then, one of the sinks of the outer binary is substituted with an inner binary of the same mass of the substituted sink. The centre of mass of the inner binary follows the orbit of the substituted sink. The subroutine devoted to this task can be called as much times as needed, in order to build a generic hierarchical system, even with more than three stars. After the initial setup, the N-body dynamics of the system is solved as described in section 2.8.5 in Price et al. (2018).

Additional information and technical details can be found in the online PHANTOM documentation: https://phantomsph.readthedocs.io/en/latest/hierarchicalsystems.html

This paper has been typeset from a TEX/LATEX file prepared by the author.